

## VESSEL COLLISION PROTECTION FOR CHACO CORRIENTES BRIDGE BY MEANS OF ENERGY ABSORBING DRILLED SHAFTS

Federico Pinto<sup>a</sup>, Carlos A. Prato<sup>a,b</sup>, and Pedro J. F. Huerta<sup>a,b</sup>

<sup>a</sup> *Departamento de Estructuras, F.C.E.F.yN., Universidad Nacional de Córdoba  
Casilla de Correos 916, Correo Central, Córdoba 5000. fpinto@efn.uncor.edu.*

<sup>b</sup> *SETEC S.R.L., Achával Rodríguez 35, Córdoba 5000,  
setecsrl@satlink.com, <http://www.setecsrl.com.ar>*

**Keywords:** chaco, corrientes, bridge, impact, vessel collision, energy absorption

**Abstract.** The Chaco-Corrientes Bridge, officially known as Puente General Belgrano, spans across the Paraná River; a major waterway that supports heavy fluvial traffic mainly consisting of barge tows, tanker, and container barges for cargo exports from Argentina, Paraguay and Brazil. Barge tow configurations can weigh up to 20,000 metric tons and displace at velocities of up to 5.3 m/s downstream. Given the fact that existing bridge piers were not designed to resist vessel impacts, and that the existing collision protection system presents several maintenance and reliability issues, a new protection system consisting of groups of drilled shafts was designed. This protection system provides a flexible energy absorbing mechanism whereby the kinetic energy of the vessels is transformed into plastic work of the protection structure. This paper describes the nonlinear numerical model that describes the behavior of the shaft group in terms of absorbed energy for head-on and oblique impacts. Given the fact that energy is absorbed through large displacements (on the order of 10 m), the model is able to consider geometric changes and second order effects on the shafts due to the weight of the cap. A simplified dynamic model that describes the head-on collision process, through which the time variation of energy transfer is studied, is also described.

**Resumen.** El puente General Belgrano, que vincula las ciudades de Resistencia (Chaco) y Corrientes sobre el río Paraná, soporta un importante tráfico fluvial consistente principalmente en trenes de barcasas de contenedores para exportación desde Argentina, Paraguay y Brasil. La masa de los conjuntos de barcasas que circulan típicamente alcanzan las 20,000 toneladas, y las mismas se desplazan a una velocidad de 5.3 m/s respecto del puente. Dado que las pilas del puente no fueron diseñadas para resistir el impacto de estas embarcaciones, y dadas las limitaciones de mantenimiento e incertidumbre de funcionamiento de las defensas actualmente dispuestas en el mismo, se diseñaron nuevas protecciones consistentes en grupos de pilotes vinculados mediante cabezales rígidos a fines de proveer un mecanismo flexible de absorción de la energía cinética de las embarcaciones mediante trabajo de deformación plástica de la estructura de defensa. El presente trabajo describe el modelo numérico no-lineal que representa el comportamiento del conjunto de pilotes en términos de absorción de energía para impactos frontales y oblicuos. Dado que el proceso de absorción de energía se desarrolla mediante grandes desplazamientos (del orden de 10m), el modelo considera cambios geométricos y efectos de segundo orden en los pilotes debidos al peso del cabezal. Se describe además el modelo dinámico no lineal que describe el proceso de colisión frontal, a partir del cual es posible estudiar la variación temporal del proceso de absorción de energía.

## 1 INTRODUCTION

The Chaco Corrientes Bridge, inaugurated in 1973, is a 1700 m long roadway that consists of a main cable-stayed bridge with a central span of 245 m, two 163.5 m lateral spans, and viaducts. The original conceptual design was carried out by Jean Courbon in the 60s whereas the main contractor was Condotte S.p.A. The main deck is a prefabricated reinforced concrete segmental box girder, with two parallel stay cable planes, and the main piers are founded on groups of 2.0 m diameter shafts.

The Paraná River supports heavy fluvial traffic, mainly due to cargo exports from Argentina, Paraguay and Brazil, for which the risk of a vessel impacting a bridge pier is of great concern. Given the fact that the original design did not consider vessel collision forces, a protection system consisting of anchored pontoons was designed in order to protect the main and hold-down piers. This protection system works by absorbing the kinetic energy of the vessel by means of mechanical work of the anchors being dragged through the river bed. The river bed dynamics presents a considerable challenge to this system, as if the anchors are buried at a depth such that the geotechnical capacity of the anchor is greater than the axial resistance of the chain, an essentially brittle failure takes place, thus rendering the system unable to absorb further energy. Hence, this system requires heavy maintenance and its reliability has been deemed not to be in accordance with the importance of the structure being protected. In fact, in 1998, while maintenance work was underway on the bridge, a barge impacted one of the main piers, fortunately causing only minor cosmetic damage to the structure. Nevertheless, this incident helped raise awareness as to the vessel collision risk this bridge was subject to.



Figure 1: View of the Chaco Corrientes Bridge

In 2003, Dirección Nacional de Vialidad (DNV) awarded contracts for the design of new protections for the bridge. Different alternatives were explored, and a preliminary design consisting of large diameter cofferdams, backfilled with granular soils, was considered. Later assessments indicated that the scour associated with these structures would be detrimental to the existing bridge foundations, and this alternative was dismissed. In 2006, a new design, based on the then recently built protections for the Rosario Victoria Bridge was proposed. The numerical analyses performed for verifying the energy absorption of the proposed design, based on groups of drilled shafts, are described in this paper.

## 2 DESIGN BASIS FOR VESSEL COLLISION

### 2.1 Background

Vessel collision is a relatively new design aspect of bridge engineering, and the development of code provisions and regulations was heavily influenced by the catastrophic collapse of the Sunshine Skyway Bridge in the United States, State of Florida, in 1980.

The American Association of State Highways and Transportation Officials (AASHTO) issued a Guide Specification (AASHTO, 1991), where several aspects of vessel collision were discussed. At the time, several existing bridges had not been designed for vessel collision and needed to be retrofitted; hence independent protection structures were discussed at length. This document also provided guidelines for deriving design impact forces of barge and ship structures impacting against rigid objects, based on earlier works by Meir Dörnberg (1983) and Woisin (1976), originally intended for collision against lock structures and against nuclear ships, respectively.

### 2.2 Energy dissipation

The collision process of a vessel against a stationary structure is such that the kinetic energy of the vessel is almost fully dissipated through plastic work. Some residual elastic energy may be restored after the collision and a marginal portion of the energy may be radiated through wave emission in the water. The plastic work, through which the bulk of the energy is dissipated, may take place either in the barge (structure is rigid), in a protection structure (flexible structure), or in both. Given the fact that the kinetic energy must be balanced by plastic work, which is the integral of forces and displacements, the structure that suffers the collapse must either develop very large forces at limited displacements or very large displacements at a limited force magnitude. An economic design would generally tend to minimize forces to be resisted; hence a ductile mechanism able to absorb large displacements is generally warranted.

When the design assumes that energy is absorbed by plastic collapse of the vessel structure, the bridge or protection structure is to be designed to resist the time history of forces that develop during the collapse process. Since the collapse mechanism depends upon the internal structure of the vessel, there is a degree of uncertainty in the peak force that may be developed, as well as its time history variation. The dynamic aspects of the problem were not very clearly defined in the original AASHTO Guidelines, nor in its subsequent updated versions. Moreover, an interim version of the Specifications was issued in 2008 (AASHTO, 2008) where aspects that needed to be clarified were specifically pointed out. Nevertheless, recent studies by Consolazio (Consolazio et al., 2008) at the University of Florida have been able to better define impact forces and dynamic effects in structures through a comprehensive research program that involved both full-scale tests and parametric studies of several existing structures.

In the case of the Chaco Corrientes bridge, the existing structure is not able to resist the dynamic impact forces that would develop during a collision, hence an independent ductile protection system was designed in order to absorb the energy of the design vessel. The protection system designed consists of groups of drilled shafts, joined by a cap that provides a geometric protection to the bridge pier cap, such that aberrant vessels would impact the protection structure and not the pier cap. The design concept for this system considers that the kinetic energy of the vessels is fully transformed into mechanical work developed in lateral loading of the shafts.

## 2.3 Mechanical model

The mechanical work that absorbs the kinetic energy is performed by the lateral loading of a group of drilled shafts (Figure 1). The connection of the shaft heads and the cap has a significant impact on the energy dissipation mechanism, as if the connection is fixed (Figure 1a), plastic hinges form at the fixity plane of the shafts and at the connection with the cap, whereas if the connection is pinned (Figure 1b), plastic hinges only develop at the fixity plane. However, the fixed cap connection generates bending moments in the cap that need to be balanced with axial compression and uplift of the shafts, which may induce a brittle geotechnical failure. Hence, following what was adopted for the Rosario Victoria Bridge (Patsch et al., 2004), a pinned connection was designed.

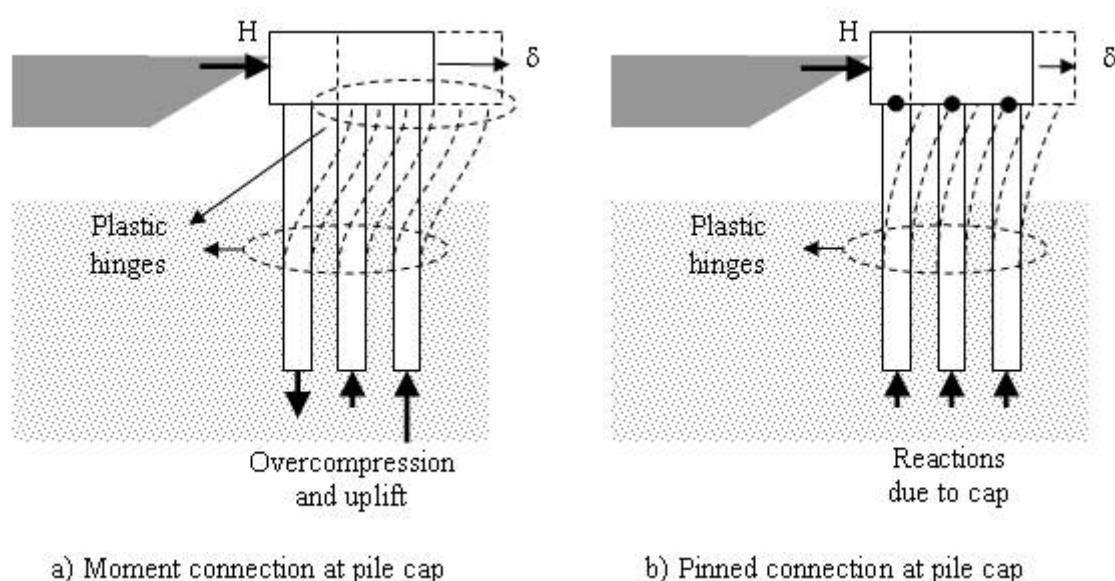


Figure 2: Mechanical model of lateral loading on protection system

The plastic hinges that develop near the fixity plane below the river bed absorb the kinetic energy of the barges and also some potential energy loss due to second order effects associated with the weight of the cap. This effect is particularly important for heavy caps and long unsupported shaft lengths.

## 3 ENERGY ABSORPTION MODEL

### 3.1 Soil model

The drilled shafts for the protection system will be founded entirely on the alluvium, which consists of medium dense to dense, poorly graded sands. Above the scour depth, these sands are loose to medium dense, whereas below scour they are medium dense to dense.

The response of the sand is modeled by means of the  $p$ - $y$  curves, which are non-linear monotonic springs that were developed by Reese and coworkers for monotonic and cyclic loading of sands (Reese et al., 1974). These nonlinear springs do not account for dynamic loading or radiation damping through the ground mass. Nevertheless, for flexible protection structures, the time history variation of forces is considered to be a low frequency, monotonic process, for which dynamic effects in the soil response may be moderate and can

conservatively be neglected in the analyses.

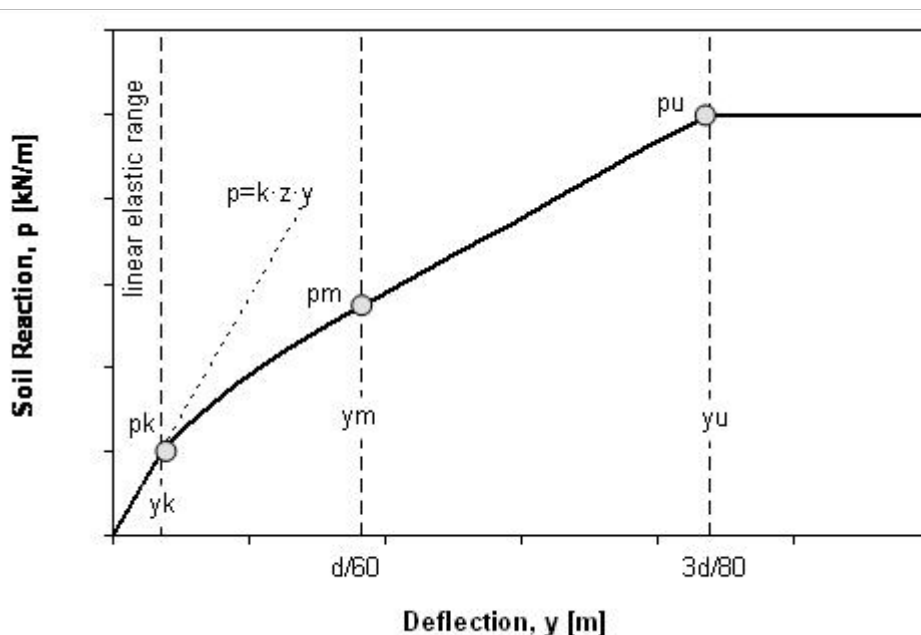


Figure 2: Nonlinear soil reaction spring model for sand (after Reese et al., 1974)

Figure 2 shows the main features of the  $p$ - $y$  curves used in the analyses, where  $p$  is the total reaction per length of the shaft,  $y$  is the lateral displacement,  $z$  is the depth at which reactions are calculated, and  $k$  is the subgrade modulus, which represents the rate of increase in elastic stiffness of the ground with depth. The nonlinear portion of the curve is defined by the friction angle,  $\phi$ , and the unit weight of the sand,  $\gamma$ . The definition of the other parameters and other calculation details can be found in Reese et al. (1974).

One important feature of these nonlinear springs is that the initial linear elastic portion of the reaction curve is variable with depth, the stiffness increasing linearly for a constant subgrade modulus,  $k$ .

In order to account for group effects, which tend to increase the displacements due to elastic interaction and also tend to reduce the ultimate lateral resistances due to overlapping plastic zones (e.g., Reese and O'Neill 1988), the  $p$ - $y$  curves were multiplied by a reduction factor (group factor). This factor, however, has very little impact in the overall analyses.

Table 1 summarizes the soil properties considered in the analyses.

Table 1: Soil properties for nonlinear spring model

Layer	$\phi$ [°]	$k$ [kN/m <sup>3</sup> ]	Group Factor
Above scour	28 to 30	10,000	0.63
Below scout	32	16,000	0.63

### 3.2 Behavior of an isolated shaft

The proposed design consists of an outer structural casing of ST 690 steel, a reinforced H38 concrete core, with ADN 420 steel reinforcement. The casing is 2.4 cm in thickness near

the plastic hinge zone and 1.0 cm some distance above the maximum moment location. A corrosion allowance of 2 mm in the steel casing was accounted for near the water surface and 1 mm near the river bed.

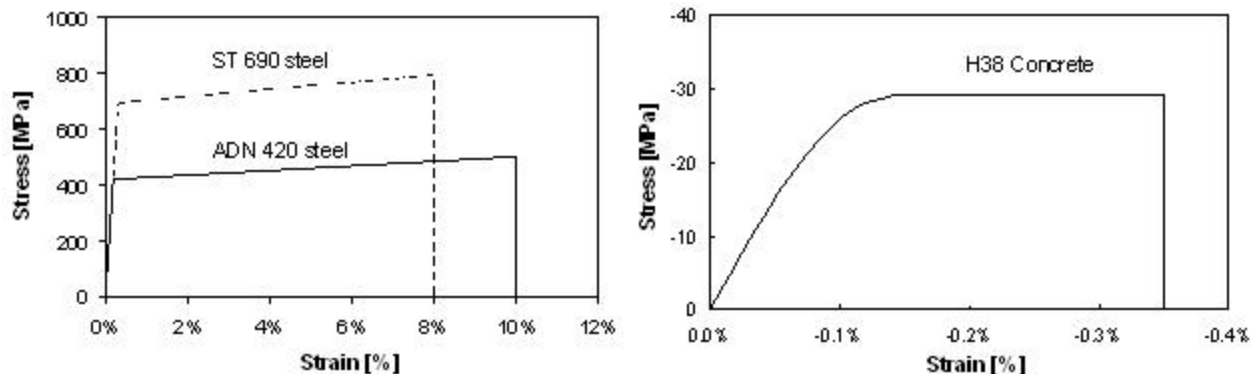


Figure 3: Stress strain curve of materials

The bending moment capacity of the shafts in the zone where the casing is 2.4 cm thick, yields 37.3 MNm, considering a reduced compressive strength of 400 MPa in the casing in order to account for possible local buckling of the outer steel.

The model considers second order moments due to axial loads on the piles. It is assumed that the weight of the cap is evenly distributed among the shafts, which is a simplifying assumption that is deemed reasonable due to the fact that all shafts are connected to a cap, thus yielding a total reaction force that may be represented by the sum of drilled shafts with average axial loads due to the weight of the cap.

Figure 4 shows results of the nonlinear numerical model of a single shaft for minimum and maximum scour conditions. It is seen that the curves reach a peak lateral load of about 2,400 and 3,600 kN for maximum and minimum scour conditions, respectively. The lateral load deflection curve presents post-peak softening due to the fact that there is a limited moment capacity at the plastic hinge, which balances both the lateral load and the second order moments due to the weight of the cap. The maximum displacement developed by the shafts is related to the limiting strain of the casing (Figure 3), which is 10% in tension. This strain is associated to a larger displacement for the maximum scour depth, since the cantilever length for this case is greater than for the minimum scour condition.

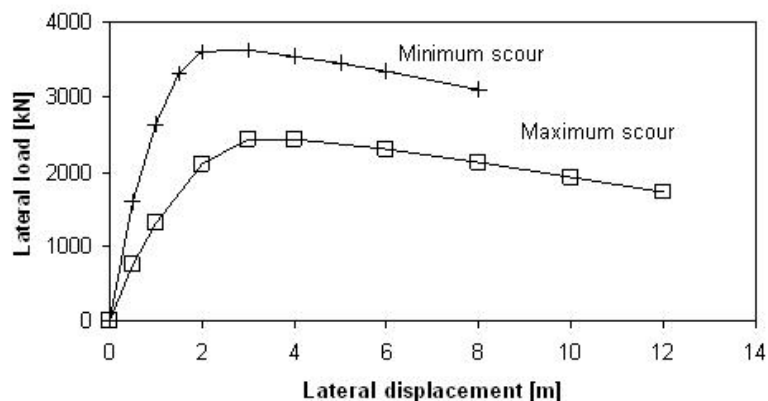


Figure 4: Load deflection curve of shafts at main pier

The energy absorbed in lateral loading by the drilled shaft is obtained as the area under the load deflection curve in Figure 4. Table 2 shows the energies absorbed for minimum and

maximum scour conditions, where it is seen that, although the lateral resistance developed for the maximum scour condition is lower than for the minimum scour, the resulting energies are similar. This is explained by fact that the maximum deflection attained is greater for the maximum scour, thus balancing the lower reaction developed. There is, nevertheless, a difference in energy, the minimum scour providing larger energy absorption. The difference is explained by the fact that some energy is lost in second order effects due to the weight of the cap, this phenomenon being more pronounced for larger unsupported lengths.

Condition	Energy [MNm]
Minimum scour	25.2
Maximum scour	23.9

Table 2: Energy absorption of single shaft at main pier location

Figure 5 shows the internal forces of the drilled shafts at maximum lateral load reaction for the maximum and minimum scour conditions. The maximum moment developed corresponds to the ultimate capacity of the cross section. It is noted that the maximum shear does not take place at the point of application of the lateral load, but at a certain depth below the river bed. Although the maximum lateral reaction is reached for the minimum scour condition, the maximum shear appears to be greater for the maximum scour condition.

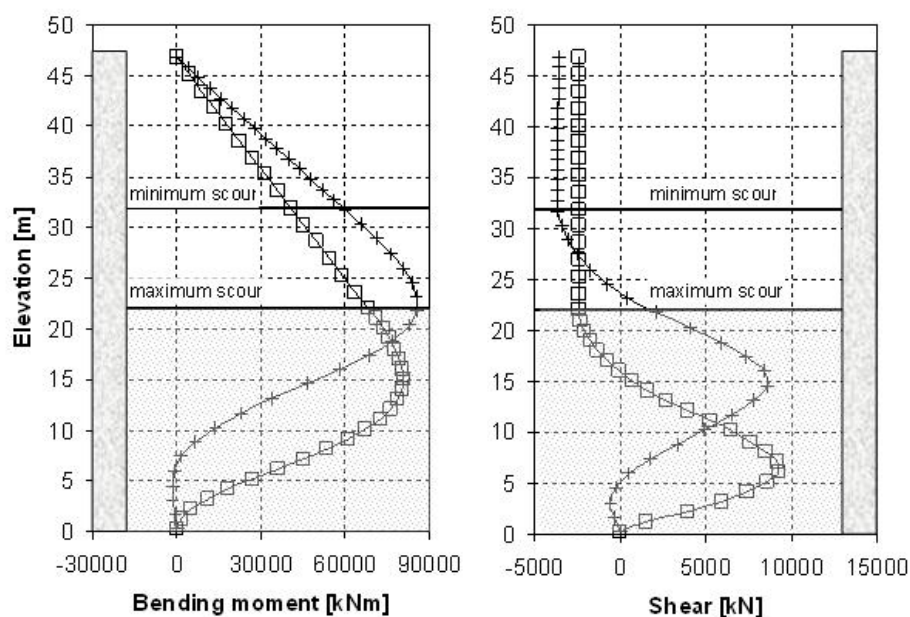


Figure 5: Internal forces in shaft for main pier locations

### 3.3 Number of shafts needed at main pier location

The energy demand is related to the kinetic energy of the vessel that may collide against the structure. Fluvial traffic studies, as well as risk analyses carried out as a part of the design effort, indicated that the design vessel consisted of a tow configuration of 4 rows of 4 Jumbo Hopper barges and tugboat (**Figure 6** and **Figure 7**). Offshore ships, which controlled the design of the Rosario Victoria Bridge 200 km downstream, are not able to navigate in the vicinity of Chaco Corrientes due to the lack of an appropriate waterway draft.

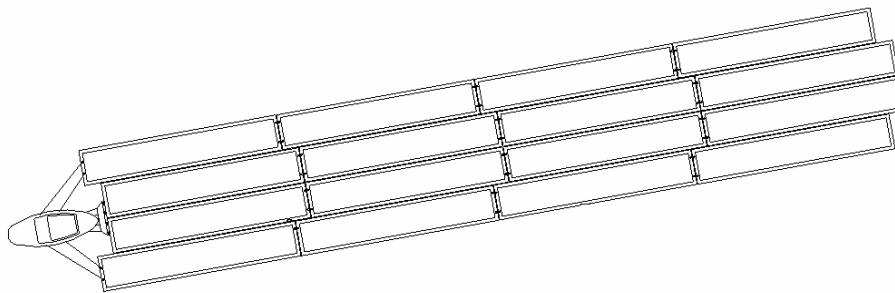


Figure 6: Design vessel: 4x4 Jumbo Hopper barge plus tugboat

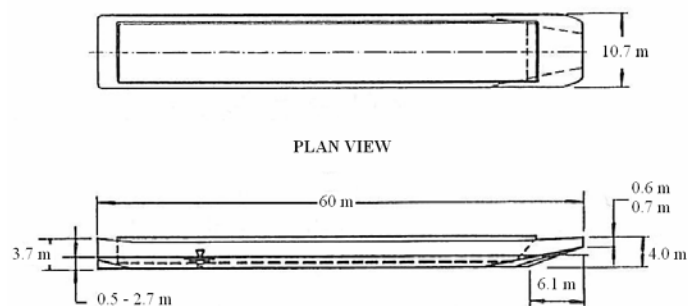


Figure 7: Jumbo hopper barge

As discussed further on in this paper, the protection structure is designed such that only the two center rows impact the protection structure head-on, whereas the two lateral rows will impact at an angle of 45 degrees. It is considered that only normal forces between barge and structure will have a large enough magnitude to effectively transfer energy. For a 45 degree angle, the square of the velocity component normal to the edge of structure is 50% of the square of the barge velocity. Hence, only 50% of the energy of the lateral rows is accounted for in the analyses. This is a reasonably conservative assumption, since it may be argued that these lateral rows may drift away after the collision of the center rows due to tension failure of the connection lashes, as suggested by the AASHTO Guidelines (2008). Nevertheless, the design considered all four rows, reducing the energy to be absorbed for the lateral rows by 50%.

The velocity of the convoy was estimated as the normal river velocity plus the relative velocity of the vessels. The total velocity was estimated at  $V=5.31$  m/sec for convoys traveling downstream in normal conditions. Thus, the total kinetic energy to be absorbed adds up to 302 MNm for the main piers.

For barge tows traveling upstream, the total velocity is the difference between the river velocity and vessel velocities.

## 4 PROPOSED DESIGN

### 4.1 Number of shafts per pier location

**Table 3** shows energy absorption calculations for each pier location, both upstream and downstream of the bridge. Design energies at downstream locations correspond to upstream velocities, and vice versa. **Table 3** also shows the number of shafts needed at different locations. It is seen that the main piers need 13 shafts for vessel collision protection.

Pier	Downstream velocity [m/s]	Upstream velocity [m/s]	Number of barge rows	Energy absorbed upstream [MNm]	Energy absorbed downstream [MNm]	Number of shafts upstream	Number of shafts downstream
3	4.06	2.13	1	59	16	3	-
4	4.46	2.50	1	71	22	4	-
5	5.31	3.29	3	302	116	14	5
6	5.31	3.29	3	302	116	14	5
7	4.46	2.50	1	71	22	4	-
8	4.06	2.13	1	59	16	3	-

Table 3: Energy absorption at different pier locations

## 4.2 Pile Caps

There are two aspects for the proposed design of the protection system; one related to the geometric protection of the pier and another related to the response of the drilled shafts. This second aspect of the design, described earlier on this paper, is based on the protections of the Rosario Victoria Bridge, which consists of steel-encased large diameter shafts, with a pinned connection at the cap. However, the geometry of the protection for Chaco-Corrientes differs significantly from the Rosario-Victoria design, due to the fact that the latter were designed for offshore ships, therefore requiring much greater number of shafts (28 for the main piers). Thus, the size of the cap in Rosario Victoria was mainly governed by the number of shafts to be accommodated, whereas in Chaco Corrientes the size of the cap was dictated by the size of the structure to be protected.

In order to maximize the protected front, and to provide a shape that would help divert aberrant vessels from potential collision courses against the protected pier, a triangular configuration with a rounded front was adopted.

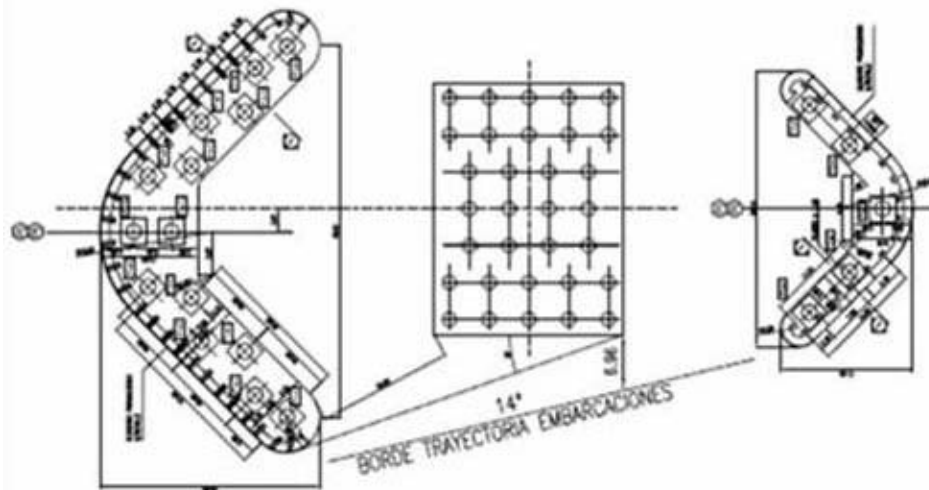


Figure 8: Proposed design at main pier

## 5 ANALYSIS OF OBLIQUE IMPACTS

The response of the shaft group to head-on impacts is trivial due to the fact that the cap is symmetric. Thus, in this case, the load deflection behavior of the group mimics that of the single shaft (Figure 4), the total reaction being simply the sum of all individual reactions.

On the other hand, given the configuration of the cap, where shafts are spread apart in an open configuration with reduced torsion stiffness, concerns were raised as to the ability of the system to absorb energy during oblique impacts. Thus, a numerical procedure was devised in order to perform quasi-static pushover analysis of the shaft group, accounting for second order effects in axial loading, as well as large displacements in the cap and nonlinear response of soil.

For the case of oblique impacts, it is considered that the barge tow is likely to be aberrant, for which the velocity normal to the sides of the cap is considered to be 50% of the velocity assumed for head-on collisions.

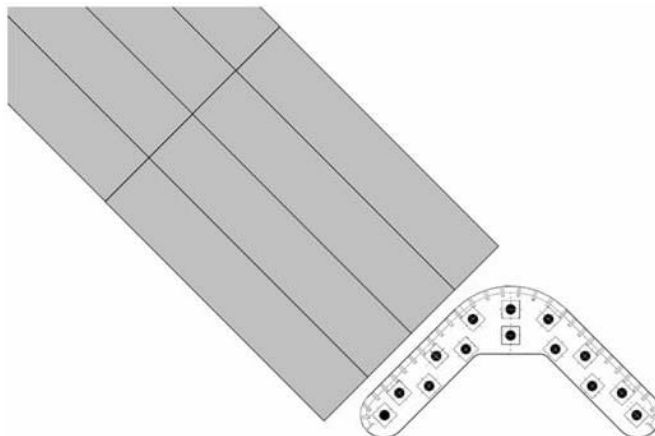


Figure 9: Assumed oblique impact

Pier	Head-on Impact			Oblique impact		
	Number of barge rows	Downstream kinetic energy [MNm]	Upstream kinetic energy [MNm]	Number of barge rows	Downstream kinetic energy [MNm]	Upstream kinetic energy [MNm]
3	1	59	-	1	15	-
4	1	71	-	1	18	-
5	3	302	116	4(upstream) 3(downstream )	101	29
6	3	302	116	4(upstream) 3(downstream )	101	29
7	1	71	-	1	18	-
8	1	59	-	1	15	-

Table 4: Energy demands in head-on and oblique impacts

## 5.1 Assumptions

The model considers each individual shaft as a nonlinear spring, whose constitutive law obeys the response of a single shaft.

For each shaft, the resultant displacement is calculated and used in order to determine the reaction in the same direction of the displacement. This reaction is then decomposed in order to obtain the reaction along the Cartesian coordinates of the model.

Second order effects due to axial loading of shafts are implicitly accounted for in the response of each individual shaft, and its effect is to reduce the lateral reaction for larger displacements.

The impact force due to the barge tow is represented by a resultant, whose magnitude is given by the reaction of the shaft group, and its direction is predetermined but its point of application along the shaft group edge varies as the group is displaced from its original position (Figure 10).

The cap is assumed to be rigid; hence displacements of all shafts are constrained and may be represented by two global displacements and a rotation, i.e., 3 degrees of freedom.

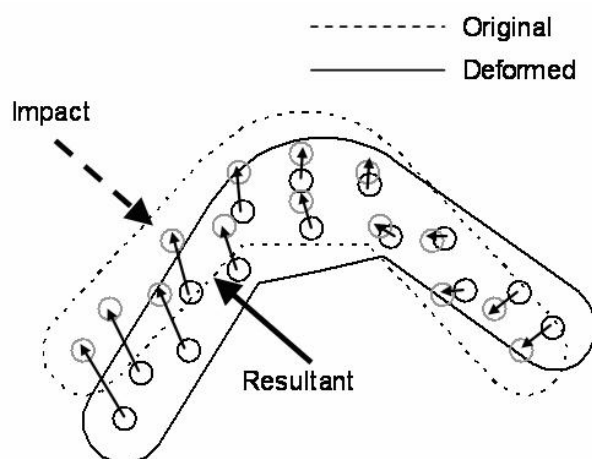


Figure 10: Equilibrium in deformed shape

## 5.2 Numerical procedure

Since large displacements are accounted for, the deformed configuration is defined by updating the coordinates of the shafts, whereas the coordinate system is stationary. Thus, the coordinates for shaft  $k$  at calculation step  $n+1$ ,  $(x_1^k, x_2^k)_{n+1}$  are defined in terms of those of step  $n$ , and the displacement increments:

$$\begin{aligned} (x_1^k)_{n+1} &= (x_1^k)_n + U_1 + r_n^k (\cos(\alpha_n^k + U_3) - \cos(\alpha_n^k)) \\ (x_2^k)_{n+1} &= (x_2^k)_n + U_2 + r_n^k (\sin(\alpha_n^k + U_3) - \sin(\alpha_n^k)) \end{aligned} \quad (1)$$

where  $\dot{U}_i$  are the incremental displacements along coordinate  $i$  and  $r_n^k, \alpha_n^k$  are the polar coordinates for shaft  $k$  at step  $n$ . The global displacement vector,  $\mathbf{U}$ , contains the global translations,  $U_1$  and  $U_2$ , and the global rotation of the cap.

The displacement increments at each shaft location are obtained as a function of the global displacements:

$$\begin{aligned} \dot{u}_1^k &= \dot{U}_1 + r_n^k (\cos(\alpha_n^k + \dot{U}_3) - \cos(\alpha_n^k)) \\ \dot{u}_2^k &= \dot{U}_2 + r_n^k (\sin(\alpha_n^k + \dot{U}_3) - \sin(\alpha_n^k)) \end{aligned} \quad (2)$$

The relationship between incremental displacements,  $\dot{\mathbf{U}}$ , and incremental force,  $\dot{\mathbf{F}}$ , is given by the tangent stiffness matrix, which is obtained as the gradient of the resultant of shaft reactions with respect to the global displacements:

$$\left(\mathbf{Kt}_{i,j}\right)_n = \sum_k \frac{\partial \left(\mathbf{R}_i^k\right)_n}{\partial \dot{U}_j} \quad (3)$$

where  $\mathbf{R}_i^k$  is the reaction (forces or moment with respect to the center of coordinates) of shaft  $k$  along the  $x_i$  coordinate, and  $U_j$  is the global displacement (or global rotation) along the  $x_j$  coordinate. The shaft reactions are obtained as a function of the total displacement:

$$\mathbf{R}_n^k = f\left(\delta_n^k\right) \quad (4)$$

$$\delta_n^k = \sqrt{\left[\left(x_1^k\right)_n - \left(x_1^k\right)_0\right]^2 + \left[\left(x_2^k\right)_n - \left(x_2^k\right)_0\right]^2} \quad (5)$$

The function  $f$ , which evaluates shaft reactions as a function of total displacements is given by the response of a single shaft (Figure 4). The direction of the reaction is defined along the opposite direction of the total displacement of the shaft. Hence, the reaction components are given by:

$$\left(\mathbf{R}_i^k\right)_n = -\frac{\left(u_i^k\right)_n}{\delta_n^k} f\left(\delta_n^k\right) \quad (6)$$

It is worth noticing that some of the mainstream commercial software packages for analysis of pile groups consider nonlinear soil springs along orthogonal directions, as opposed to considering the nonlinear reactions along the total displacement components. This leads to increased resistances, as the available capacities along the orthogonal directions may geometrically be summed up. This shortcoming was avoided in the analyses presented here, as resultant displacements are used in order to calculate resultant reactions, which are later decomposed in order to obtain the Cartesian components of the shaft reactions.

By combining equations 2 to 6, the tangent stiffness matrix, which yields symmetrical, is derived analytically.

The basic procedure for the nonlinear integration of the equations of motion is based on evaluating the change in global displacements due to a change in the applied resultant force. Given the fact that softening of the shafts is possible due to second order effects (Figure 4), the increment of force is selected such that the resulting work yields a set positive value (e.g., Bathe, 1996). Thus, the increment of external load is defined as:

$$\dot{\mathbf{P}}_n = \lambda_n \mathbf{F} \quad (7)$$

where  $\mathbf{F}$  is a vector containing the components of the external load for a unit magnitude, thus being a function of the direction of the load and distance with respect to the center of coordinates. The  $\lambda$  multiplier is obtained by means of the tangent stiffness matrix, such that the resulting work increase equals a prescribed value:

$$\dot{W} = \dot{\mathbf{U}}^T \mathbf{P}_n = \lambda_n \mathbf{F}^T (\mathbf{Kt})_n^{-1} \mathbf{P}_n \quad (8)$$

$$\lambda_n = \frac{\dot{W}}{\mathbf{F}^T (\mathbf{Kt})_n^{-1} \mathbf{P}_n} \quad (9)$$

The increase in global displacements is then estimated as:

$$\dot{\mathbf{U}} = (\mathbf{Kt})_n^{-1} \lambda_n \mathbf{F} \quad (10)$$

This estimation is used in order to determine displacements and reactions in the deformed

configuration. The resultant vector of all individual shaft reactions would generally mildly deviate from the prescribed direction of the load. Therefore, a correction force vector, normal to the prescribed direction of the external load, is evaluated and used in order to adjust the global displacement vector until the resultant of the individual shaft reactions falls in the prescribed direction of the external load within a certain degree of accuracy. Thus, the actual load increase (or decrease) resulting from each calculation step is given by the actual shaft reactions in the deformed configuration, whereas the load multiplier in equation 9 is only used as an initial estimate.

Figure 11a shows the load deflection curves of the protection structures at the main pier locations for the design scour conditions and considering head-on as well as oblique impacts. The displacements in Figure 11a correspond to the cumulative displacement at the point of application of the external load, which is not necessarily a fixed point along the side of the cap but may vary along the direction of the impact during the collision process. As noted before, the curve for the head-on case mimics the load deflection curves for single shafts. As seen in Figure 11a, for the head-on collision case, the shafts are assumed to quickly lose lateral capacity after a total displacement of 12 m due to tension failure of the casing steel.

For the case of oblique impacts, a sharp decline in reaction load may be seen in Figure 11a after a displacement of 8-m along the point of application of the impact load. This is due to the fact that some shafts within the cap are undergoing displacements greater than 12-m, thus losing lateral capacity at a fast rate.

Figure 11b shows the energy absorbed, in terms of mechanical work of the external load, as a function of maximum cap displacements for both head-on and oblique impacts. The displacements for the head-on collision are uniform within the cap, whereas they reach a maximum at the end of the cap close to the impact force, as seen in Figure 12.

The maximum displacements are of importance due to the fact that the protection structure must not come into contact with the pier cap, in order to prevent any lateral load transfer to the main structure, which was not designed for such a loading case. The displacements obtained in the analyses are 10.7 m for the head-on and 8.3 m for the oblique collision cases.

The numerical analyses considered a target work increment,  $\dot{W} = 10\text{MNm}$ , and an unbalanced force tolerance of 1kN, which represents 0.05% of a total peak reaction of 20 MN. Nevertheless, the load multiplier was kept within a range where  $-100 < \lambda < 1000$ , in order to limit the load increment and help faster convergence.

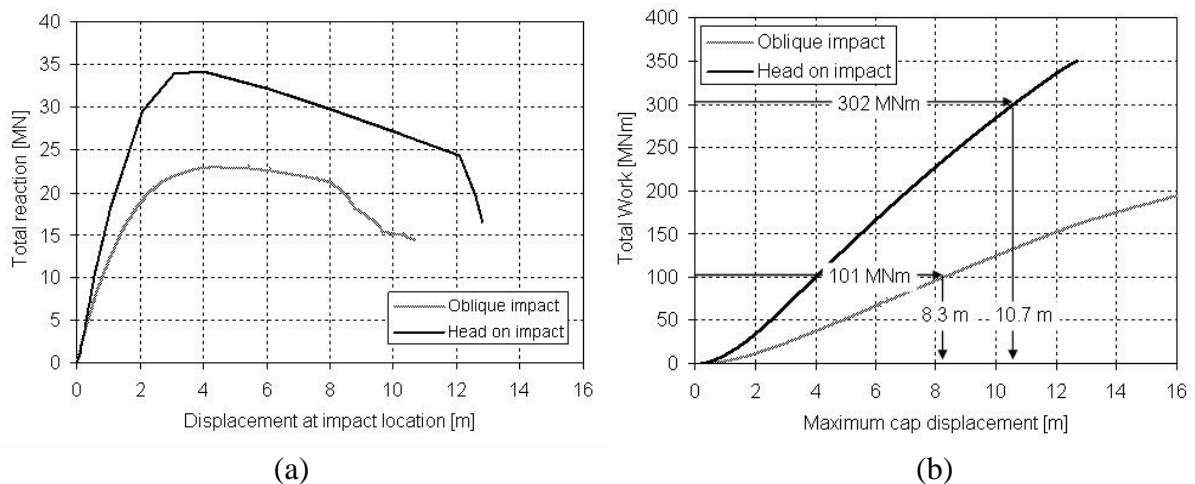


Figure 11: Load deflection and energy absorption at main pier location

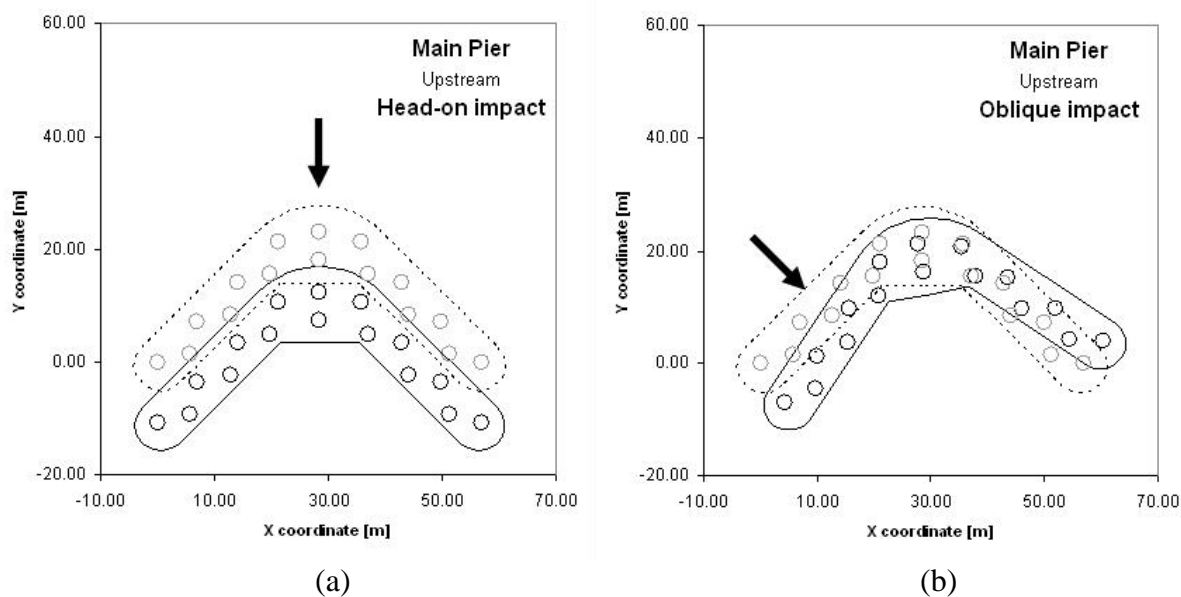


Figure 12: Deformed configuration at design energy

## 6 DYNAMIC ANALYSIS OF ENERGY TRANSFER

The preceding analyses consider that the kinetic energy of the vessels is fully absorbed by mechanical work of the drilled shafts. Nevertheless, energy may be absorbed in several other mechanisms present in the collision phenomenon, namely; nonlinear crushing behavior of barge bow, radiation of waves through soil and water, etc. Also, the preceding analyses do not account for the dynamic phenomenon, whereby a massive structure (caps weigh up to 3000 metric tons) is suddenly impacted by a moving mass. Hence, in order to study the overall process of energy transfer, a simplified model was developed in order to represent a dynamic head-on collision.

### 6.1 Simplified model

Figure 13 shows a layout of the simplified model considered for the analyses. The model considers the barge tow and pile cap as a single longitudinal mass, whereas the bow and drilled shaft reactions are modeled by means of nonlinear longitudinal springs. Hence, the only source of damping in the system corresponds to the nonlinear hysteretic behavior of the barge bow and drilled shafts.

The mathematical model is thus described by means of two degrees of freedom: displacement of the barge tow,  $u_B$ , and displacement of the pile cap,  $u_C$ .

The drilled shaft springs are reversible, meaning that they provide reactions for displacements of the cap along both directions, whereas the bow spring only provides reactions along the direction contrary to the initial velocity of the barge (i.e., cap towards barge). The bow reactions are also zero for cases where  $u_B < u_C$ , i.e., when cap moves more than the barge tow.

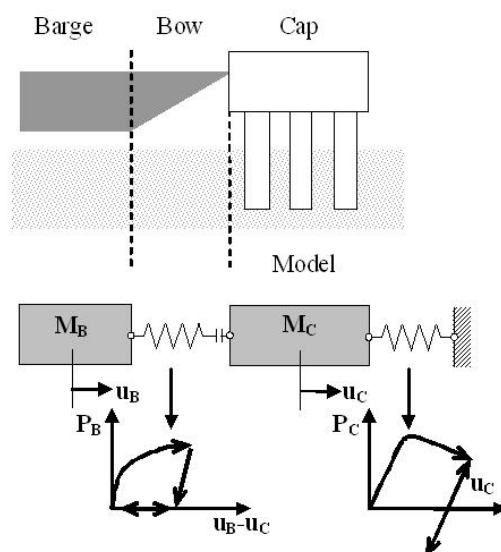


Figure 13: Simplified model for dynamic analysis

The nonlinear behavior of the drilled shaft springs has been described earlier on this paper, and the spring is defined in Figure 11a for the head-on collision case.

## 6.2 Simplified barge bow behavior

The load-deflection behavior of barge bows has been a topic of considerable research, both experimental and analytical, at the University of Florida in the recent years (e.g., Consolazio and Cowan, 2003, Consolazio et al., 2005). As of 2008, AASHTO recommendations are, however, based on reduced scale experiments by Meir-Dörnberg (1983). These earlier experiments consisted of dynamic and static loading by means of pendulum hammers, as well as analytical computations. Results were cast in terms of “equivalent static forces”, meaning that the forces measured during the experiments in both static and dynamic conditions did not differ significantly. Nevertheless, several authors (e.g., Yuan, 2005, Consolazio et al., 2008) noted that the term “equivalent static” may be misleading, as engineers may assume that the load already accounts for dynamic amplification of the impacted structure, which is certainly not the case.

Figure 14 shows load deflection curves for a Jumbo Hopper barge bow given by AASHTO LRFD (2008) and Consolazio and Cowan (2003) for rounded piers. The Consolazio and Cowan curves show an initial stiffness and yield load lower than AASHTO’s recommendations. It is also noted that, whereas AASHTO indicates a progressively increasing load, Consolazio and Cowan show an almost constant average value for the post-yield loading range. It should be noted that Consolazio and Cowan reported results up to 0.6 m of deflection.

In order to perform simplified analyses, both AASHTO and a simplified curve, based on Consolazio and Cowan, were considered. The latter is defined as shown in Figure 14, but considering a limiting damage depth at which the load increases greatly in order to attribute a limited energy absorption capacity to the barge bow structure. Maximum damage depths of 1.0 and 2.0 m were considered, partially based on the fact that the Consolazio and Cowan data shows bow displacements up to 0.6 m. The behavior of the barge bow after the maximum damage depth was assumed elastic, with a very large stiffness in order for the load to be controlled by the protection structure, as it would be expected for a rigid object impacting a flexible structure. This is a conservative assumption, as a limit is placed to the energy that can

be absorbed by the barge, thus requiring a larger energy absorption in the protection structure itself. This assumption is also intended to reflect the uncertainty in the structural response of the barges, since little information is generally made available to bridge designers as to the actual configuration or load deflection response of these structures.

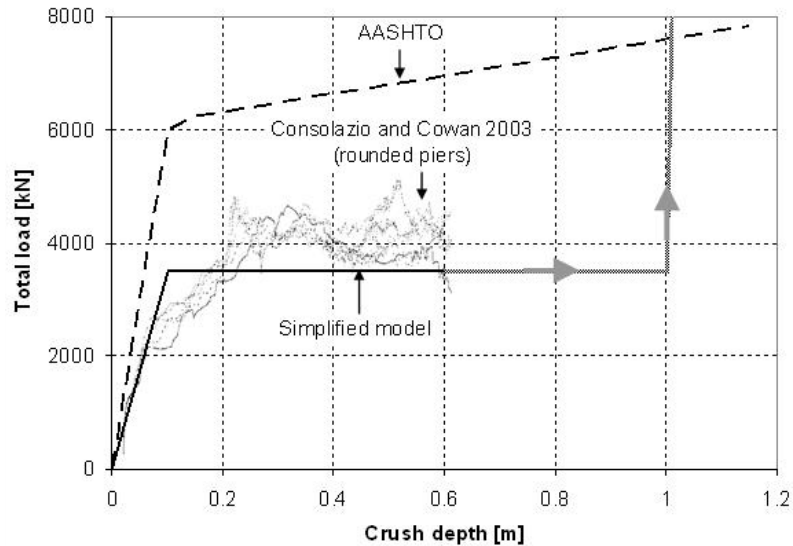


Figure 14: Load deflection behavior of barge bow

It is considered that unload-reload curves are linear and parallel to the initial stiffness. For the simplified model curves in Figure 14, it is considered that once the maximum damage is reached, the barge structure can no longer absorb additional energy, hence the reload path follows an elastic reload-unload path with a large stiffness, as shown in **Figure 15**.

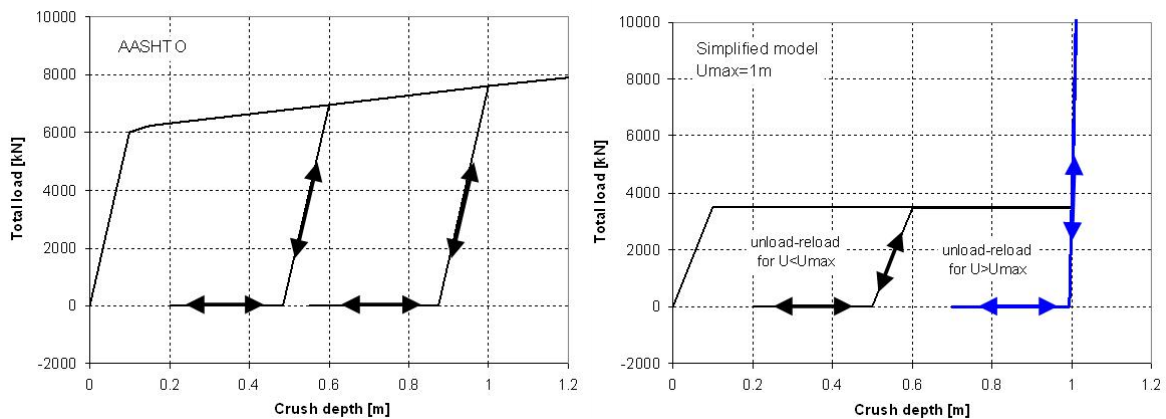


Figure 15: Assumed bow behavior in unloading-reloading

As described earlier in this paper, 4 rows of barges are considered for the head-on collision case, with a 50% reduction on the demands of the two lateral rows. The same approach is followed in order to determine the total bow spring, i.e., the values shown in **Figure 14** are multiplied by a factor of three in order to account for the full barge tow.

### 6.3 Numerical analysis

The equations of motion, expressing dynamic equilibrium along the longitudinal direction for the simplified model shown in Figure 13 are as follows:

$$\begin{aligned} F_B(u_B - u_C) &= M_B \ddot{u}_B \\ F_C(u_C) - F_B(u_B - u_C) &= M_C \ddot{u}_C \end{aligned} \quad (11)$$

where  $F_B$  and  $F_C$  are the bow and cap reactions, which are functions of the crush depth,  $u_B - u_C$ , and cap displacement,  $u_C$ , respectively. The initial conditions are zero initial displacements, and an initial velocity of the barge equal to 5.31 m/s. A numerical solution of equations 11 is obtained by considering an explicit scheme:

$$\begin{aligned} u_B^{k+1} &= 2u_B^k - u_B^{k-1} + F_B(u_B^k - u_C^k) \frac{\Delta t^2}{M_B} \\ u_C^{k+1} &= 2u_C^k - u_C^{k-1} + [F_C(u_C^k) - F_B(u_B^k - u_C^k)] \frac{\Delta t^2}{M_C} \end{aligned} \quad (12)$$

Given the fact that an explicit scheme is used, the time increment is governed by the large stiffness assigned to the bow spring after the maximum displacement is reached. This stiffness is set at value of 10 times the initial bow stiffness, and the time step is set to less than 10% of the lowest natural period of the barge-cap system considering the largest stiffness values for cap and bow.

#### 6.4 Results

Figure 16 shows barge and cap displacement histories for different bow behavior assumptions. It is seen that the overall trends for barge displacements are similar, with a residual upstream velocity that reflects the portion of elastic energy stored in the drilled shaft group and barge bow. The cap displacement somewhat differ for the different bow assumptions, with a maximum value of 10.4 m for the simplified and 8.2 m for the AASHTO bow behavior cases. The free vibrations that may be observed for  $t > 6$  sec show an identical natural frequency for all assumptions, as it is only a function of the elastic stiffness for the drilled shaft group and cap mass.

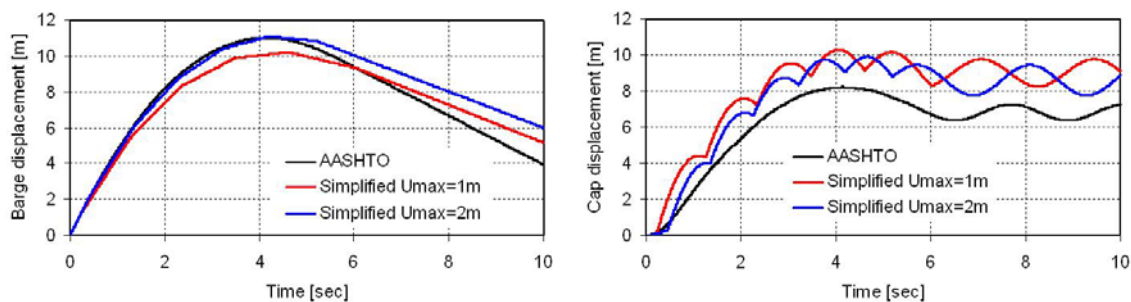


Figure 16: Barge and cap displacement histories

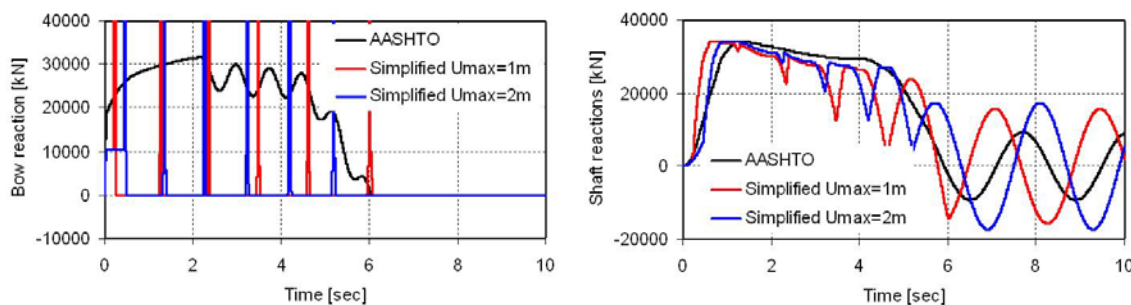


Figure 17: Bow and drilled shaft reaction histories

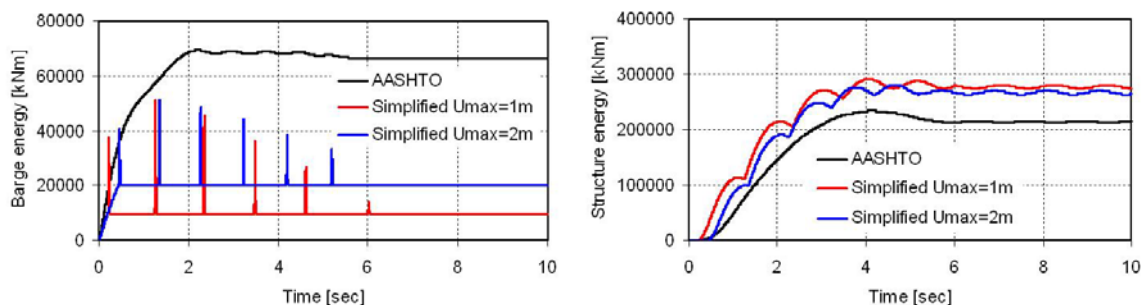


Figure 18: Barge and drilled shaft energy absorption histories

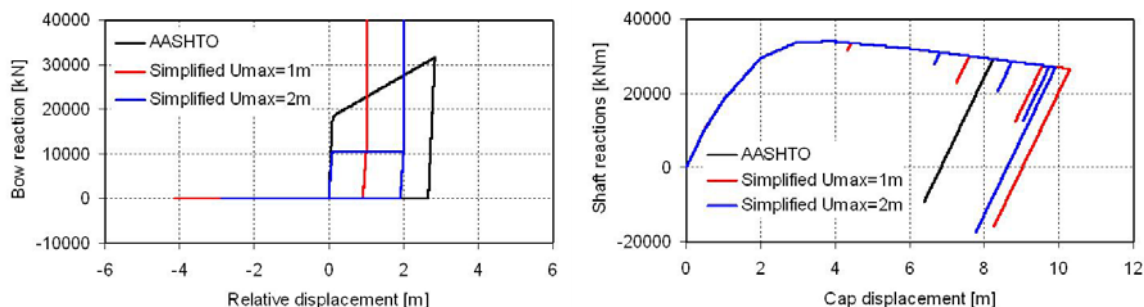


Figure 19: Bow and drilled shaft reactions vs. displacements

Figure 17 shows bow and shaft reaction histories, where several spikes in load are seen for the simplified bow behavior curves, due to the limiting damage assumption, whereby the load increases greatly after a certain crushing depth has been reached. It is also seen that, after the first spike in load, the reactions are either zero or very large, which is consistent with the assumptions described earlier. Interestingly, the maximum reaction of the drilled shaft group is very similar for all different bow behavior assumptions.

**Figure 18** shows time histories of energy absorption for both barge bow and protection structures. The energy spikes observed for the simplified bow behavior assumptions reflect the elastic energy stored for damage depths greater than the limited values. Since elastic behavior is assumed after the limiting damage value, these energy spikes are quickly restored to the system and are not permanently absorbed by the bow structure.

It is seen that AASHTO's bow behavior assumption yields significant energy absorption on the barge, with a final value of 70 MNm out of a total initial kinetic energy of 302MNm (i.e., 23%). However, for the simplified assumption cases, more than 93% of the energy is dissipated through plastic work in the drilled shaft group.

Given the fact that the protection structure is able to dissipate the full initial kinetic energy of the barge tow, AASHTO's bow assumption could suggest that the number of drilled shafts provided in the design could be reduced. However, given the uncertainties in actual barge bow behavior, and in order to accommodate possible larger demands in future vessel traffic, it was decided not to reduce the number of drilled shafts in the design.

**Figure 19** shows load displacement (or damage) curves for bow and protection structures, where it is seen that a maximum bow damage of 3 m is obtained for the AASHTO bow behavior case, whereas the damage is limited to 1 and 2 m for the other simplified assumptions.

## 7 CONCLUSIONS

A new vessel collision protection system for the Chaco-Corrientes Bridge, consisting of energy absorbing drilled shafts, has been designed. The design is based on the protection structures already built for the Rosario-Victoria Bridge, 200 km downstream over the Paraná River.

The design required numerical analyses in order to verify the performance of the protection structure for head-on as well as oblique impact conditions. The analyses results were instrumental in verifying that energy was absorbed in a ductile manner, whereas maximum calculated displacements were considered in order to provide a sufficient clearance between the protection and bridge structures. Analyses showed that the protection system provides a softer response for oblique impacts. Nevertheless, as the energy demand for oblique impacts is reduced, the maximum displacements were of similar magnitudes as for head-on collisions.

Simplified nonlinear dynamic analyses were performed in order to assess the energy absorption contribution of the barge bow considering several load-damage behavior assumptions. By considering the AASHTO load-damage curve, it was found that the bow structures could dissipate about 23% of the total initial kinetic energy of the barge bow, whereas other load-damage assumptions showed that the bulk of the energy (i.e., more than 93%) was absorbed by the protection structure. At the time this effort was undertaken (2006), it was decided not to take advantage of the energy that could be absorbed in the barge bow for the final design, hence the protection structures were designed to fully absorb the kinetic energy of the barge tow. Nevertheless, the energy absorption capacity of the barges could be taken advantage of for future protection structure designs for bridges in the Paraná River, thus reducing the number of shafts and associated costs for these structures.

## 8 REFERENCES

- AASHTO, Guide Specification and Commentary for Vessel Collision Design of Highway Bridges, American Association of State Highway and Transportation Officials, Washington, D.C., 1991.
- AASHTO LRFD Bridge Design Specifications, Customary U.S. Units, 4th Edition, with 2008 Interim Revisions. American Association of State Highway and Transportation Officials, Washington, D.C., 2008.
- Bathe, K. J., Finite Element Procedures, Prentice-Hall, 1996.
- Consolazio, G.R. and Cowan, D.R.. Nonlinear analysis of barge crush behavior and its relationship to impact resistant bridge design. *Computers and Structures*, 81(8-11), pp. 547-557, 2003.
- Consolazio, G. R., Cowan, D. R., Biggs, A., Cook, R. A., Ansley, M., and Bollmann, H. T. Full-Scale Experimental Measurement of Barge Impact Loads on Bridge Piers. *Journal of the Transportation Research Board*, Transportation Research Record, No. 1936, pp. 81-93, 2005.
- Consolazio, G. R., McVay, M. C., Cowan, D. R., Davidson, M. T., Getter, D. J., Development of Improved Bridge Design Provisions for Barge Impact Loading. Structures Research Report 2008/51117, University of Florida, Civil and Coastal Engineering, Gainesville FL, April 2008.
- Meir Dörnberg, K. E., Ship Collisions, Safety Zones, and Loading Assumptions for Structures in Inland Waterways, Association of German Engineers, Report No. 496, 1983.
- Patsch, A., Gerbaudo, C. F., Prato, C. A. Analysis and Testing of Piles for Ship Impact Defenses, *Journal of Bridge Engineering*, ASCE, Volume 7, Issue 4, pp. 236-244, July/August 2002.
- Reese, L. C., Cox, W. R., and Koop, F.D. Analysis of Laterally Loaded Piles in Sand, *Proceedings*, Offshore Technology Conference, Houston, Texas, Vol. II, 1974.
- Reese, L. C., and O'Neill, M. W. Drilled Shafts: Construction Procedures and Design Methods. , Federal Highway Administration, FHWA-HI-88-042, Washington, D.C, 1988.
- Woisin, G. The Collision Tests of the GKSS. Yearbook of the Shipbuilding Technology Society, Vol. 70, pp. 465-487, Berlin, 1976.
- Yuan, P. Modeling, Simulation and Analysis of Multi-Barge Flotillas Impacting Bridge Piers. PhD Dissertation, University of Kentucky, College of Engineering, Lexington, KY, 2005.